ations and note some possible physical applications. The Coulomb field intensity inside the sphere is typically non-zero: the angular components (E_ϑ and E_φ) vanish along the symmetry axes, but the radial component (E_ρ) does not (see Fig. 1). Note that $E_\rho \to 0$ at the centre; the size of the approximately null region increases with N, eventually leading to the continuous classical limit (zero field everywhere).

According to classical electrostatics[6], a charge Nq uniformly smeared on the surface of a sphere has potential $V = Nq/R$ on and inside the sphere. In the discrete case, however, this expression holds true only at the centre: elsewhere, V is different (see Fig. 1). Also, V exhibits a marked directional dependence; potentials along some directions are reminiscent of some phenomenological potentials used in nuclear physics: hollow spheres, charge concentrated at the origin, volume-charged spheres[21] and truncated Coulomb potentials[22-24].

The discrete energy form-factor w is significantly lower than the classical limits for surface-charged (0.5) and volume-charged (0.6) spheres[21] (see Tables 1, 2). This may have implications for semi-empirical nuclear-mass formulae for light nuclei, and for nuclear radii[25].

Let the effective surface of the discrete configuration be defined as the locus ρ^* where V attains a maximum along a particular direction; its shape is not spherical, as illustrated in Fig. 2. In head-on collisions between particles of charge Q and stationary discrete configurations, the apparent surface depends on the initial energy of the projectile. This surface steadily shrinks with increasing energy until the hard-core (ρ^*) obtains. A suitable averaging procedure on ρ^* may lead to an equivalent radius for rotating systems (possible connections: nuclear radii[25,26], proton hard-core, nuclear scattering). A remarkable fact in Fig. 2 is that $\rho^* = 0$ along some directions. This implies that the configuration may be transparent to a charged particle travelling with non-relativistic energy $K > NqQ/R$ (with q and Q of the same sign). If the configuration is rotating, there is still a finite probability that the particle may appear undisturbed at the other side of the system (possible connections: nuclear scattering). The converse phenomenon is *classical tunnelling*; that is, the possibility that a charge Q originally at rest in the centre of the sphere (unstable equilibrium) may escape along some preferred directions, appearing at infinity with kinetic energy $K = NqQ/R$ (possible connections: radioactive decay).

The two-dimensional symmetry of stable nested polygons (Table 1) is quite remarkable (possible connections: two-dimensional crystal growth processes, as in snowflakes[27-29]). The energetically favourable three-dimensional configurations in Table 2 often exhibit non-pentagon symmetries ($N = 20$ is noteworthy); even the icosahedron, paradigm of 5-fold symmetry, may be described as two-nested triangular antiprisms[14] as shown in Table 2 (possible connections: three-dimensional crystals).

We thank A. A. Berezin, O. Knop, N. M. Queen and our colleagues B. Sigg, K. Tichy and G. Yadigaroglu for comments and suggestions.

Received 29 October 1985; accepted 11 February 1986.

1. Berezin, A. A. *Nature* **315,** 104 (1985).
2. MacGowan, D. *Nature* **315,** 635 (1985).
3. Nityananda, R., Cormack, A. M., Naumann, R. A. & Webb, S. *Nature* **316,** 301-302 (1985).
4. Queen, N. M., Rees, M. & Berezin, A. A. *Nature* **317,** 208 (1985).
5. Aspden, H. *Nature* **319,** 8 (1986).
6. Jeans, J. H. *The Mathematical Theory of Electricity and Magnetism* 5th edn, 36, 42 (Cambridge University Press, 1933).
7. Morse, P. M. & Feshbach, H. *Methods of Theoretical Physics* Vol. 1, 201 (McGraw-Hill, New York, 1953).
8. Leech, J. *Mathl Gaz.* **41,** 81-90 (1957).
9. Fejes Toth, L. *Regular Figures*, 102-123, 157 (Pergamon, Oxford, 1964).
10. Coxeter, H. S. M. *Regular Polytopes*, 33-57 (Methuen, London, 1948).
11. King, R. B. *J. Am. chem. Soc.* **92,** 6455-6466 (1970).
12. Melnyk, T. W., Knop, O. & Smith, W. R. *Can. J. Chem.* **55,** 1745-1761 (1977).
13. Fejes Toth, L. *Am. J. Math.* **70,** 174-180 (1948).
14. Whyte, L. L. *Am. math. Mont.* **59,** 606-611 (1952).
15. Foppl, L. *J. reine angew. Math.* **141,** 251-302 (1912).
16. Goldberg, M. *Maths Comput.* **23,** 785-786 (1969).
17. Cohn, H. *Mathl Tabl. natn. Res. Counc., Wash.* **10,** 117-120 (1956).
18. Lin, Y. C. & Williams, D. E. *Can. J. Chem.* **51,** 312-316 (1973).
19. Claxton, T. A. & Benson, G. C. *Can. J. Chem.* **44,** 157-163; 1730-1731 (1966).
20. Britton, D. *Can. J. Chem.* **41,** 1632-1634 (1963).
21. Evans, R. D. *The Atomic Nucleus*, 32-39 (McGraw-Hill, New York, 1955).
22. Singh, D., Varshni, Y. P. & Dutt, R. *Phys. Rev.* **A32,** 619-622 (1985).
23. Patil, S. H. *Phys. Rev.* **A24,** 2913-2919 (1981).
24. Mehta, C. H. & Patil, S. H. *Phys. Rev.* **A17,** 43-46 (1978).
25. Hefter, E. F. *Phys. Rev.* **A32,** 1205-1027 (1985).
26. Elton, L. R. B. *Nuclear Sizes* (Oxford University Press, 1961).
27. Maddox, J. *Nature* **313,** 93 (1985).
28. Mortley, W. S. *Nature* **313,** 638 (1985).
29. Schrack, R. A. *Nature* **314,** 324 (1985).

Lunar nodal tide and distance to the Moon during the Precambrian

James C. G. Walker* & Kevin J. Zahnle*†

* Department of Atmospheric and Oceanic Sciences, and
† Department of Astronomy, The University of Michigan, Ann Arbor, Michigan 48109, USA

The pace of tidal evolution for the past ~450 Myr implies an Earth/Moon collision some 1,500–2,000 Myr BP (see ref. 1), an event for which there is no corroborating evidence. Here we present the first direct determination of the lunar distance in the Precambrian. We interpret a 23.3 ± 0.3-yr periodicity preserved in a 2,500 Myr BP Australian banded iron formation (BIF)[2] as reflecting the climatic influence of the lunar nodal tide, which has been detected with its modern 18.6-yr periodicity in some modern climate records[3-10]. The lunar distance at 2,500 Myr BP would then have been about 52 Earth radii. The implied history of Precambrian tidal friction is in accord with both the more recent palaeontological evidence and the long-term stability of the lunar orbit. The length of the Milankovitch cycles that modulate the ice ages today[11-13] also evolve with the Earth–Moon system. Their detection in the Precambrian sedimentary record would then permit an independent determination of the lunar distance.

Evidence for the rate of lunar recession is available on several different timescales. As these matters have been discussed in detail elsewhere[1,14,15], we shall discuss them only briefly here. Direct determination by laser ranging yields a recession velocity $\dot{a} \simeq 1.1 \times 10^{-7}$ cm s^{-1} (ref. 16), where a refers to the lunar distance. The amplitudes and phases of the various tides can be inferred from their influences on satellite orbits, from which $\dot{a} \simeq 1.2 \times 10^{-7}$ cm s^{-1} (ref. 16) is calculated. Over longer periods, lunar occultation timings and the historical record of total solar eclipses imply that $\dot{a} \simeq 1.3 \times 10^{-7}$ cm s^{-1} over the past few millenia[1].

The most important source of long-term information derives from fossil corals and molluscs[1,17]. In brief, fine laminae are interpreted either as daily growth increments or as the record of the semidiurnal or diurnal tide, in accordance with the general growth habits of their modern descendants. Modulation of the fine banding by the fortnightly or monthly tidal cycles and by the yearly seasonal cycle allows estimates of the number of days per year, the number of days per month, and the number of months per year. Lambeck's preferred solution, obtained by considering a filtered set of the palaeontological data and additionally imposing conservation of angular momentum for the Earth–Moon system, may be expressed as $\dot{a} \simeq 9.5 \times 10^{-8}$ cm s^{-1}. Scrutton's evaluation of the palaeontological data is essentially identical[17].

The quality of the palaeontological record declines abruptly when looking back into the Precambrian. The only previously exploited data come from stromatolites. However, stromatolites

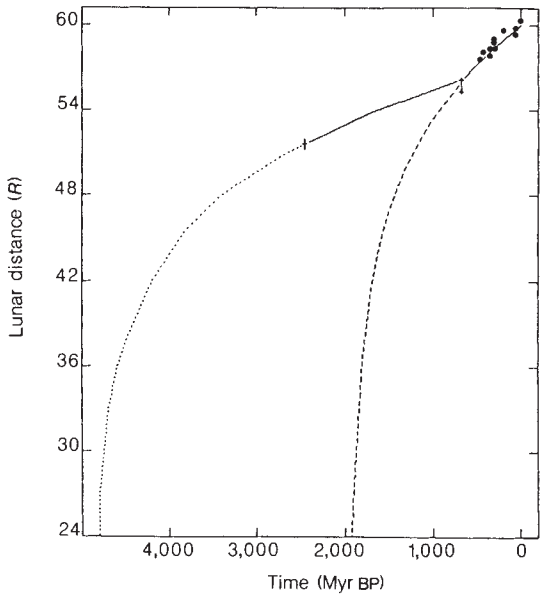

Fig. 1 Radius of the lunar orbit (in units of R, the Earth radius) through Earth's history. The Phanerozoic data are adapted from ref. 17. The Precambrian datum has been deduced from a 23.3-yr periodicity preserved in the Weeli Wolli banded iron formation, which we have identified with the lunar nodal tide. Dashed curve, an extrapolation [equation (3)] based solely on the Phanerozoic data; dotted curve [equation(5)] presumes an average Precambrian tidal torque consistent with both the palaeontological data (●) and the Weeli Wolli datum (+).

do not appear to be good timekeepers today, and the correct interpretation of ancient stromatolitic data is far from obvious[1,17].

Precambrian inorganic sources of periodic banding do exist; however, since inorganic processes are comparatively slow, observable periodicities must be relatively long. The most interesting of these was found by Trendall[2] in the Weeli Wolli Formation of the Hamersley Group in Western Australia[18]. Here it suffices to note that the Weeli Wolli is a banded iron formation dating from ~2,450 Myr BP. The finest bands (or 'varves') are believed to be annual[2,18]. The varves themselves vary cyclically with a period of 23.3 ± 0.3 yr, counted over 23 complete cycles. The absence of a readily discernible 11-yr cycle led Trendall to doubt that the 23.3-yr cycle is in fact the 22-yr Hale (double-sunspot) cycle.

We tentatively interpret the 23.3-yr cycle as a consequence of the climatic impact of the lunar nodal tide. The lunar nodal tide, presently 18.6 yr, appears weakly in some modern climate records. It arises from the precession of the moon's orbital plane about the ecliptic. It has been detected in temperature and rainfall records in western North America[3-5] and eastern Australia[5], and in tree-ring data from both western North America[4,6] and Patagonia[7]. It has also been detected in the Indian monsoons[8,9] and perhaps in Beijing's rainfall[10] (a claim disputed by Clegg and Wigley[19]) and Nile River flooding[20].

What is most important from our present perspective is that this period depends on the Earth/Moon distance. The lunar nodal period may be conveniently expressed as[21]

$$P = P_0\left[\frac{\cos I_0}{\cos I}\right]\left(\frac{a_0}{a}\right)^{1.5} \tag{1}$$

where the modern values are $P_0 = 18.6$ yr, $a_0 = 3.84 \times 10^{10}$ cm, and $I_0 = 5.15°$, which is the inclination of the lunar orbit to the ecliptic.

Interpreted as the lunar nodal period, the 23.3-yr cycle places the Moon at $a/a_0 = 0.86 \pm 0.01$. When plotted in comparison with the modern rate of tidal dissipation (Fig. 1), it is clear that this is about where the Moon should have been at that time if the catastrophic close approach is to be averted.

Neglecting the solar tide and the inclination and eccentricity of the Moon's orbit, the recession of the Moon due to the semidiurnal tide may be written after Lambeck[1] as

$$\dot{a} = Aa^{-11/2} = \langle\dot{a}_0\rangle\left(\frac{a}{a_0}\right)^{-11/2} \tag{2}$$

where

$$A = \tfrac{3}{16}(1+\cos(i))^4 \frac{GmR^5 k_2}{(G(M+m))^{0.5}} \sin\delta$$

and where $\langle\dot{a}_0\rangle$ is the average velocity of lunar recession at $a = a_0$; i the inclination of lunar orbit to Earth's Equator (23.5° today); R and M the radius and mass of Earth; m the lunar mass; G the gravitational constant; and k_2 and δ the equivalent Love number and phase lag of the tide. Assuming that A is constant (equivalent to assuming that tidal energy dissipation is directly proportional to the total tidal energy; that is, assuming a constant Q factor), equation (2) is readily integrated:

$$\frac{a}{a_0} = \left[1 - \tfrac{13}{2}T\frac{\langle\dot{a}_0\rangle}{a_0}\right]^{2/13} \tag{3}$$

where T is time measured back from the present. In terms of T:

$$T = \tfrac{2}{13}\frac{a_0}{\langle\dot{a}_0\rangle}\left[1 - \left[\frac{a}{a_0}\right]^{13/2}\right] \tag{4}$$

For a lunar recession velocity $\langle\dot{a}_0\rangle = 1 \times 10^{-7}$ cm s^{-1}, an Earth/Moon collision is indicated 1,900 Myr ago (Fig. 1). As we have only the single datum for the first ~4,000 Myr of Earth history, deriving a single Precambrian tidal dissipation rate to go with the single Phanerozoic rate is as much analysis as can be justified. An equation matching the Precambrian datum to equation (3) is:

$$\frac{a}{a_0} = \frac{a_1}{a_0}\left[1 - \tfrac{13}{2}(T - T_1)\frac{\langle\dot{a}_1\rangle}{a_1}\right]^{2/13} \tag{5}$$

where

$$\langle\dot{a}_1\rangle = 0.30\langle\dot{a}_0\rangle\left[\frac{a_1}{a_0}\right]^{-11/2} = (0.43)\langle\dot{a}_0\rangle$$

and where T_1 refers to the nominal boundary between the Precambrian and the Phanerozoic. Hence, the average tidal friction (relative to the forcing) in the Proterozoic was ~30% that in the Phanerozoic. Tidal friction in the Archaean, although no larger, may have been lower still. This rate of tidal dissipation is consistent with the stability of the lunar orbit, as shown in Fig. 1.

The Milankovitch cycles of ~23, ~41 and ~105 kyr are periodicities of Earth's orbital parameters that have a prominent role in modulating the ice age climate[12,13]. The longest period is in the magnitude of the eccentricity[22,23], which should be constant over the life of the Solar System. By contrast, both the 41-kyr ('obliquity') and the 23-kyr ('precession') cycles depend in part on the precession of Earth's polar axis with respect to the fixed stars (precession of the equinoxes)[22,23], which results from lunar and solar torques on Earth's equatorial bulge. Its period may be written as[24]

$$P_{\text{eqnx}} = 25{,}800\left[\frac{\Omega_0}{\Omega}\right]\left[\frac{\cos\gamma_0}{\cos\gamma}\right]\left[\frac{1.465}{(a_0/a)^3 + 0.465}\right] \text{yr} \tag{6}$$

where γ is the average obliquity of the polar axis, and Ω the rotation angular velocity. For the present argument, we neglect the small evolutionary change in cos γ (ref. 25), and we assume that the Earth/Moon system angular momentum is constant, so

that P_{eqnx} may be written entirely in terms of a:

$$P_{eqnx} = 37{,}800\left[\left\{5.87 - 4.87\left(\frac{a}{a_0}\right)^{0.5}\right\}\left\{\left(\frac{a_0}{a}\right)^3 + 0.465\right\}\right]^{-1} \quad (7)$$

Since P_{eqnx} varies not only as a function of lunar distance but also as a function of the daylength through its impact on the equatorial bulge, it is possible, in principle, to determine the daylength directly.

The period of obliquity oscillations may be written as

$$P_{obl} = \left[\frac{1}{P_{eqnx}} - \frac{1}{P_{incl}}\right]^{-1} \quad (8)$$

where $P_{incl} = 68.8$ kyr for the most important term[24].

The perihelion precession is composed of four larger terms and a myriad of smaller ones[22,23]. These may be written in the form

$$P_{peri} = \left[\frac{1}{P_{eqnx}} + \frac{1}{P_{ecc}}\right]^{-1} \quad (9)$$

where the most important eccentricity periods are 308, 176, 72.6 and 75.3 kyr (ref. 23). These correspond to P_{peri} of 23.7, 22.4, 19 and 19.2 kyr, respectively.

The amplitude of the obliquity oscillation also varies[24]. This may be written approximately as

$$\Delta\gamma = 2.0° \frac{P_{eqnx}}{P_{incl} - P_{eqnx}} \quad (10)$$

As there are in fact half a dozen other periods associated with non-negligible, albeit lesser, inclination variations, equation (10) should really be written as a sum, the terms of which are given by Ward[24]. What is shown by equation (10) is that the magnitude of the obliquity oscillations is increasing, and that it was about 40% of its present value when the Weeli Wolli Formation was laid down.

We conclude that the Milankovitch periodicities that might be expected in the Weeli Wolli Formation or another formation of comparable age would be ~105, ~17 and ~13 kyr, respectively. The shorter of these might be associated with the alteration between BIF bands and S bands reported by Trendall[18] for the Dales Gorge Member of the Brockman iron formation.

This research was supported in part by NASA grant NAGW-176.

Received 6 November 1985; accepted 20 January 1986.

1. Lambeck, K. *The Earth's Variable Rotation* (Cambridge University Press, New York, 1980).
2. Trendall, A. F. *Econ. Geol.* **68**, 1089-1097 (1973).
3. Currie, R. G. *J. geophys. Res.* **86**, 11055-11064 (1981).
4. Currie, R. G. *J. geophys. Res.* **89**, 1295-1308 (1984).
5. Vines, R. G. *J. geophys. Res.* **87**, 7303-7311 (1982).
6. Currie, R. G. *J. geophys. Res.* **89**, 7215-7230 (1984).
7. Currie, R. G. *Geophys. Res. Lett.* **10**, 1089-1092 (1983).
8. Campbell, W. H., Blechman, J. B. & Bryson, R. A. *J. Clim. appl. Met.* **22**, 289-296 (1983).
9. Currie, R. G. *Geophys. Res. Lett.* **11**, 50-53 (1984).
10. Hameed, S., Yeh, W. M., Cess, R. D. & Wang, W. C. *Geophys. Res. Lett.* **10**, 436-439 (1983).
11. Hays, J. D., Imbrie, J. & Shackleton, N. J. *Science* **1294**, 1121-1132 (1976).
12. Crowley, T. J. *Rev. Geophys.* **21**, 828-877 (1983).
13. Lorius, C. *et al. Nature* **316**, 591-596 (1985).
14. Brosche, P. & Sündermann, J. (eds) *Tidal Friction and the Earth's Rotation* (Springer, New York, 1978).
15. Brosche, P. & Sündermann, J. (eds) *Tidal Friction and the Earth's Rotation* Vol. 2 (Springer, New York, 1982).
16. Cazenave, A. in *Tidal Friction and the Earth's Rotation* Vol. 2 (eds Brosche, P. & Sündermann, J.) 4-18 (Springer, New York, 1982).
17. Scrutton, C. T. in *Tidal Friction and the Earth's Rotation* (eds Brosche, P. & Sündermann, J.) 154-196 (Springer, New York, 1978).
18. Trendall, A. F. in *Iron Formations: Facts and Problems* (eds Trendall, A. F. & Morris, R. C.) 69-129 (Elsevier, New York, 1983).
19. Clegg, S. L. & Wigley, T. M. L. *Geophys. Res. Lett.* **11**, 1219-1222 (1984).
20. Hameed, S. *Geophys. Res. Lett.* 843-845 (1984).
21. Kaula, W. M. *An Introduction to Planetary Physics* (Wiley, Toronto, 1969).
22. Berger, A. *Astr. Astrophys.* **51**, 127-135 (1976).
23. Berger, A. *J. atmos. Sci.* **35**, 2362-2367 (1978).
24. Ward, W. R. *Icarus* **50**, 444-448 (1982).
25. Goldreich, P. *Rev. Geophys.* **4**, 411-439 (1966).

Sahel rainfall and worldwide sea temperatures, 1901–85

C. K. Folland, T. N. Palmer & D. E. Parker

Meteorological Office, London Road, Bracknell RG12 2SZ, UK

Using the comprehensively quality-controlled Meteorological Office Historical Sea Surface Temperature data set (MOHSST)[1,2] we show for the first time that persistently wet and dry periods in the Sahel region of Africa are strongly related to contrasting patterns of sea-surface temperature (SST) anomalies on a near-global scale. The anomalies include relative changes in SST between the hemispheres, on timescales of years to tens of years, which are most pronounced in the Atlantic. Experiments with an 11-level global atmospheric general circulation model (AGCM) support the idea that the worldwide SST anomalies modulate summer Sahel rainfall through changes in tropical atmospheric circulation[3–6]. El Niño events may also play a part. We do not discount the effects of soil moisture and albedo changes in the Sahel[7,8], although Courel *et al.*[9] have questioned the importance of albedo changes, but we do suggest that worldwide SST anomalies may have a more fundamental influence on Sahel rainfall.

Rainfall records for sub-Saharan North Africa have been collated and normalized by many authors. We have used an

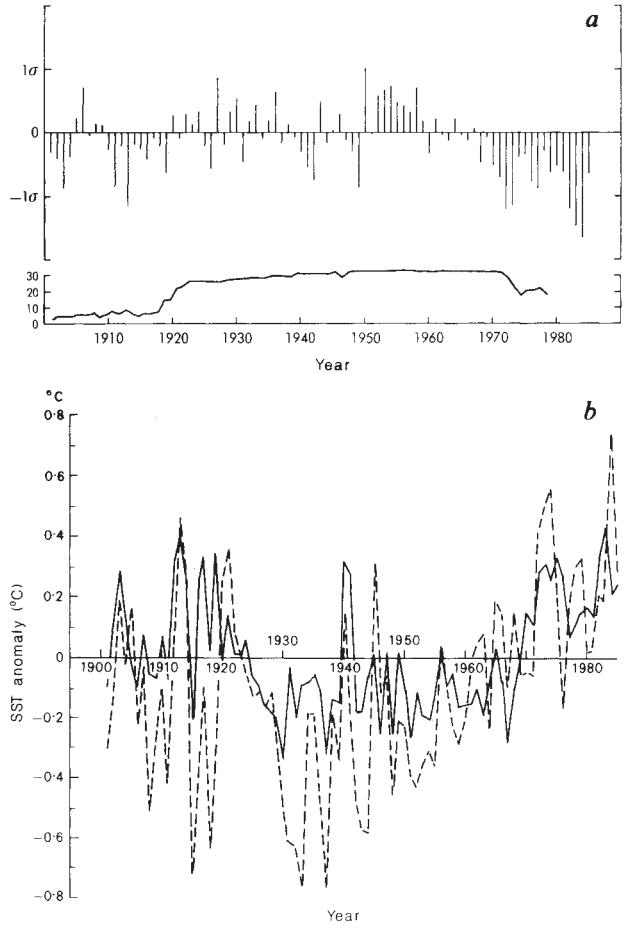

Fig. 1 *a*, Standardized annual rainfall anomalies for the Sahel, 1901-85 (upper panel). Values to 1984 are after Nicholson[11]; 1985 values are from CLIMAT reports. The lower panel gives the numbers of stations used. *b*, SST anomalies (relative to 1951-80), for July to September 1901-85. Solid line, Southern Hemisphere with the Northern Indian Ocean, minus the rest of the Northern Hemisphere (SHNI − RNH). Dashed line, South Atlantic minus North Atlantic.